Characterization of friction behavior under cryogenic conditions: Ti–6Al–4V☆

Achraf Fersi *, Yessine Ayed, Bruno Lavisse, Guénaël Germain

Arts et Metiers Institute of Technology, LAMPA, F-49035, Angers, France

Keywords:
Tribology
Cryogenic condition
Friction coefficient
Titanium
Adhesion
Numerical simulation

A B S T R A C T

Friction phenomena at the chip/tool/workpiece interfaces during machining of material impacts significantly the cutting process. In this article, the effect of friction conditions (dry, emulsion, cryogenic) on the tribological performance of uncoated tungsten carbide tools is investigated when machining titanium alloy Ti–6Al–4V. Friction tests were conducted to analyze the impact of sliding speed and cooling on the evolution of the friction coefficient. To determine the real friction coefficient (adhesive friction coefficient), a numerical simulation using the Lagrangian method was employed. After a comparative study of various simulation methods (“Lagrangian”, “CEL”, and “ALE”), the Lagrangian method was identified as the most relevant. The obtained results reveal that an increase of sliding velocity significantly influences the friction coefficient. Additionally, the application of cryogenic fluid (LN2) reduces the friction coefficient compared to both dry and emulsion-based friction. Adhesion phenomena play a crucial role in the nature of the contact, especially at high sliding velocities.

1. Introduction

The use of titanium alloys holds significant importance in various industries, particularly for high-value components. These alloys exhibit exceptional mechanical properties, including corrosion resistance, fatigue endurance, and a high strength-to-weight ratio, even at elevated temperatures. They are extensively used across various sectors such as aerospace, automotive production, petrochemicals, and medical industries, Du et al. [1] and Arab et al. [2]. However, machining titanium alloys remains challenging due to their low thermal conductivity and strong chemical reactivity with cutting tool materials. These factors result in elevated temperatures at the tool tip during machining, thereby accelerating tool wear. The heat generated during machining remains localized at the tool edge, subjecting it to critical thermomechanical loads [3]. Consequently, effective cooling strategies are necessary to reduce the cutting zone temperature. Various cooling fluids, such as emulsions (water + oil), have been employed for this purpose, but their efficacy remains limited. Alternatively, the use of cryogenic fluids, such as liquid nitrogen (LN2), offers significantly improved cooling performance and minimizes tool wear [4,5].

Wear zones primarily result from the friction between the tool and chip, as well as the tool and workpiece, both of which significantly impacts tool life. Therefore, understanding the tribological interactions between the tool and the machined material remains a crucial focal point for researchers. Several studies such as Bogdan-Chudy et al. [6], Uçak et al. [7], Basten et al. [8] and Schulze et al. [9] focus on the tribological behavior in machining, aiming to understand the physical phenomenon at the cutting zone and optimize the simulation of cutting process. Courbon et al. [10] tested a sphere-cylinder configuration for Ti–6Al–4V and WC/Co friction. The authors concluded that the friction coefficient was unchanged for dry contact, as well as under the influence of both liquid nitrogen and gaseous nitrogen. The results of Pušavec et al. [11], indicate that the projection of LCO2 leads to increase the friction coefficient. Nevertheless, when coupled with oil (LCO2 + oil), it decreases the friction coefficient by 80%. The researchers concluded that not only the materials of cutting tool and workpiece have an important effect on the friction coefficient [12], but also the nature of the machining process [13] and the cooling/lubrication conditions [14].

This study aims to investigate the impact of sliding speed and various friction conditions (dry, emulsion, and cryogenic environments) on the tribological behavior of Ti–6Al–4V with tungsten carbide tools. Friction tests were conducted under extreme machining conditions,

☆ This document is the results of the research project funded by the Cetim, the Carnot ARTS Institute and the Pays de la Loire Region and Angers Loire Métropole.

* Corresponding author.
E-mail addresses: achraf.fersi@ensam.eu (A. Fersi), yessine.ayed@ensam.eu (Y. Ayed), lavisse.bruno@ensam.eu (B. Lavisse), guenael.germain@ensam.eu (G. Germain).

https://doi.org/10.1016/j.triboint.2024.109588

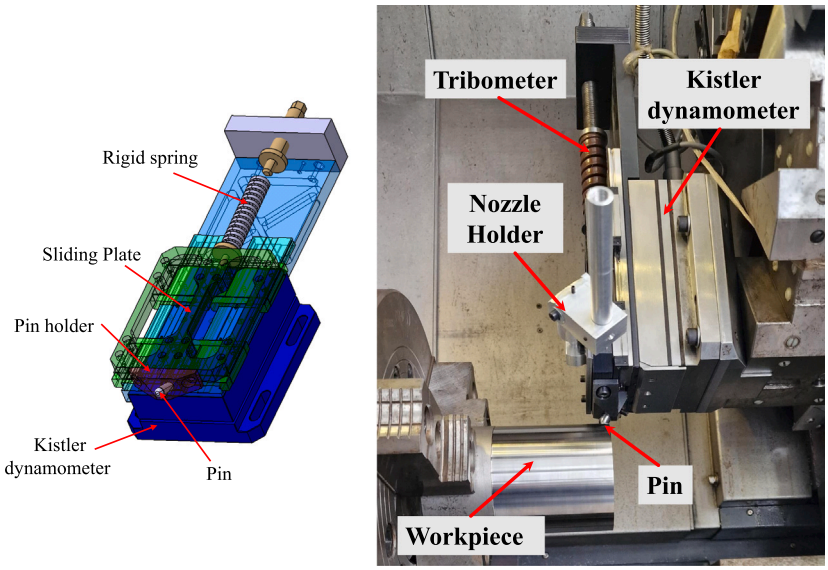

Fig. 1. Tribometer device.

characterized by high sliding speeds and very high contact pressure, to observe the evolution of the friction coefficient and to analyze tribological phenomena. Numerical simulation is essential for decoupling these phenomena and accurately determining the real friction coefficient. Additionally, a specific study was carried out to implement a relevant numerical simulation.

2. Tribometer and friction test

The investigation into material tribological behavior is characterized by conducting experimental friction tests using a tribometer. In this particular study, these tests were carried out employing an open tribometer developed at the LAMPA laboratory, as illustrated in Fig. 1. Its design was inspired from previous works such as Zemzemi et al. [15] and Abdelali et al. [16]. The fundamental principle of this device is to apply a normal force (F_N) via a spherical-tipped pin to a rotating cylindrical part. The normal force is applied using a spring mechanism, ensuring consistent contact pressure between the pin and the workpiece throughout the duration of the experiment.

In this study, tribological tests were conducted using a Leadwell LTC25iL CNC lathe. The Ti–6Al–4V workpiece was fixed onto the rotating chuck of the lathe. The rotation speed (N) was set to establish the desired sliding speed (V_g), while the carbide pin feed was maintained at 0.5 mm per revolution to prevent any overlap in the pin's path. The combination of the rotational movement of the workpiece and the pin's movement resulted in a helical groove over the entire surface. The choice of a sphere-cylinder contact configuration is justified by the objective of attaining a significant contact pressure at the pin/workpiece interface. This set-up provides the apparent friction coefficient (μ_{app}) which is calculated as the ratio between the tangential and normal forces as follow :

$$\mu_{app} = \frac{F_T}{F_N} \tag{1}$$

With F_N is the normal force and F_T is the tangential force. For measuring the normal (F_N) and tangential (F_T) forces, the tribo-system is fixed on a Kistler dynamometer (9257B).

3. Adhesive friction coefficient

The local contact between the workpiece and the pin provides two phenomena: the adhesion phenomenon (due to the friction between the two parts) and a plastic deformation generated by the pressure of the pin against the material surface as shown in Fig. 2. The plastic deformation phenomena cannot be ignored under such severe conditions, as a result the apparent friction coefficient does not characterize the real friction coefficient. Bowden and Tabor [17] proposed a decomposition of the apparent friction coefficient (μ_{app}) in two parts as:

$$\mu_{app} = \frac{F_T}{F_N} = \mu_{adh} + \mu_{plast-def} \tag{2}$$

With (μ_{adh}) is the adhesive friction coefficient and ($\mu_{plast-def}$) is the plastic deformation coefficient due to the plastic deformation in front of the pin.

The phenomenon of adhesion corresponds to the physical friction between two surfaces (It can be modeled using Coulomb's law). The adhesive coefficient thus represents the actual friction coefficient between the two solids (this is the friction coefficient introduced in the Coulomb model). The plastic deformation phenomenon upstream of the tool is due to material deformation, resulting in a tangential contact force, independent of the friction coefficient.

The proportion of each relative part varies depending on the studied materials (pin and workpiece) and the contact conditions (contact pressure, sliding speed, dry or lubricated contact, etc.). The adhesive friction coefficient (μ_{adh}) cannot be determined experimentally, it must be calculated by subtracting ($\mu_{plast-def}$) from the measured (μ_{app}). Therefore, it is necessary to simulate the friction test numerically to identify the adhesive coefficient (μ_{adh}) using an inverse method. Consequently, a numerical model has been developed to characterize local friction coefficient.

3.1. Testing conditions

The selection of friction conditions is crucial for conducting accurate friction tests. Previous studies, such as Sima and Özel [18] and Karpat [19] concluded that the contact pressure in the cutting zone during the machining of titanium (Ti–6Al–4V) with carbide tools reaches a maximum value of 1.5 GPa. The phenomenon was simulated numerically using the Abaqus code to determine the magnitude of the required normal force (F_N). The results indicated that the normal force required to maintain this value of contact pressure at the pin/workpiece interface is 350 N. The Table 1 presents the selected friction conditions across various sliding speeds (V_g). In order to ensure the repeatability of the results, each test was replicated three times. After each test, the surface was refreshed using a cutting tool.

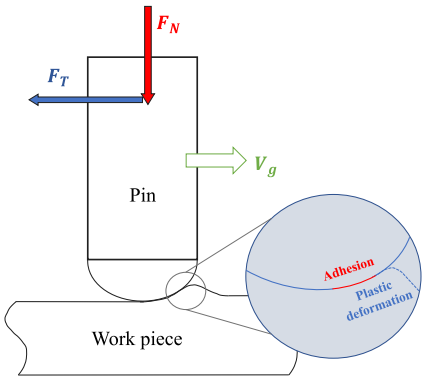

Fig. 2. Local contact [16].

Table 1
Friction conditions.

Vg (m/min)	F_N (N)
15	350
30	
45	
60	
75	
90	

Table 2
Mechanical properties of pin (WC-Co).

Propriety	Value
Density ρ (kg m^{-3})	12 800
Young's modulus E (Gpa)	630
Poisson's ratio ν	0.22
Specific heat C_p (J kg^{-1} °C^{-1})	226
Heat conductivity λ (W °C^{-1} m^{-1})	44.6

4. Numerical simulation

This section provides a detailed description of the numerical study, which aims to simulate the friction test for the identification of the adhesive friction and plastic deformation coefficients.

4.1. Description of the model

To simulate the friction test, the ABAQUS/Explicit code is employed to develop a 3D model. This model represents the constrained contact zone between the pin and the cylindrical workpiece as a sphere-plane contact. The model geometry is presented in Fig. 3. The pin is modeled with a spherical tip (⌀9 mm), while the workpiece is simulated with a parallelepiped form (4 × 3 × 2 m^3).

4.1.1. Pin

The pin is modeled by a spherical tip linked (lie) to an upper part considered as rigid. It is meshed with 819 tetrahedral (C3D4) elements with a size of 400 µm. A reference point (RP) is located above the pin to manage its displacement. The pin is made of grains of tungsten carbide (WC) bonded with cobalt, its mechanical properties are illustrated in Table 2.

4.1.2. Workpiece

The parallelepiped workpiece is meshed with C3D8R hexagonal elements. In the contact zone the elements size is set to 50 µm in order to guarantee a precise result as shown in Fig. 3. The mechanical properties of the work material are reported in Table 3.

Table 3
Mechanical properties of Ti–6Al–4V [20].

Propriety	Value
Density ρ (kg m^{-3})	4420
Young's modulus E (Gpa)	114.5
Poison's ratio ν	0.31
Specific heat C_p (J kg^{-1} °C^{-1})	580
Heat conductivity λ (W °C^{-1}m^{-1})	6.6

Table 4
Johnson–Cook parameters of Ti–6Al–4V [20].

A (MPa)	B (MPa)	n	m	T_{fus} (°C)	T_{amb} (°C)
800	743	0.3	0.7	1655	20

The mechanical behavior of the workpiece is modeled by the Johnson–Cook behavior law. It expresses stress as a function of equivalent strain, equivalent strain rate and temperature as follow:

$$\bar{\sigma} \equiv (A + B_p^n)[1 + C \ln\left(\frac{\dot{\varepsilon}_p}{\dot{\varepsilon}_{p0}}\right)][1 - \left(\frac{T - T_{\text{amb}}}{T_{\text{fus}} - T_{\text{amb}}}\right)^m] \quad (3)$$

According to the above equation, Johnson–Cook's law can be divided into three terms. The first relates to the phenomenon of strain-hardening in the material, with coefficients A, B and n. The second term relates to the dynamic hardening of the material, which varies according to the equivalent plastic strain rate. Coefficient C is a constant defining the dependence on the strain rate. The third term corresponds to thermal softening for temperature values between the initial temperature T_{amb} and the melting temperature T_{fus}. "m" is the thermal softening exponent. The values of these constants are illustrated in Table 4.

4.2. Contact behavior

The mechanical contact between the pin and the workpiece is modeled using Coulomb's law, which expresses the relationship between normal stress (σ_n) and tangential stress (τ_f) using the following equation:

$$\tau_f = \mu_{adh-num}.\sigma_n \quad (4)$$

The coefficient of adhesive friction ($\mu_{adh-num}$) is introduced into the simulation as a constant along the contact area.

4.3. Simulation approaches of friction test

The simulation of friction test was approached through various numerical methods, as mentioned in the literature. Zemzemi et al. [15,21] and Bonnet et al. [22] used the Lagrangian approach. While, Rech et al. [23], Abdelali et al. [16] and Cao [24] employed the Arbitrary Eulerian–Lagrangian (ALE) method. Notably, Fezai et al. [25] opted for the Coupled Eulerian–Lagrangian (CEL) method. In this section, these strategies were evaluated based on criteria such as results, accuracy, and computation time to determine the most suitable approach for simulating friction test.

4.3.1. Lagrangian method

In a Lagrangian analysis, the mesh nodes are attached to the material so that the material boundary coincides with the element boundary. The Lagrangian elements follow the material as it deforms. However, when the elements deform significantly, the analysis may either stop or the calculations may diverge [26,27]. The simulation of the friction test using the Lagrangian approach involves fixing the part through its base and moving the pin, as shown in Fig. 4. The simulation is divided into two steps: indentation and scratching. During the indentation step, the pin moves vertically, penetrating the material to a certain depth (h) to establish contact pressure. In the second step, the pin moves horizontally, rubbing against the contact zone with a well-defined speed (V_g).

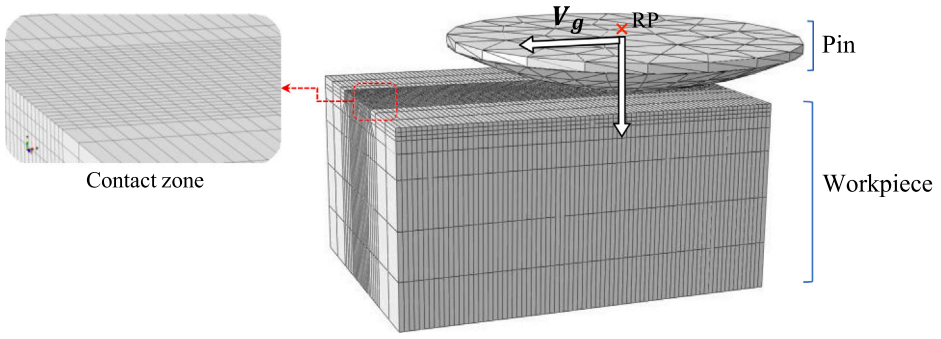

Fig. 3. Geometric model.

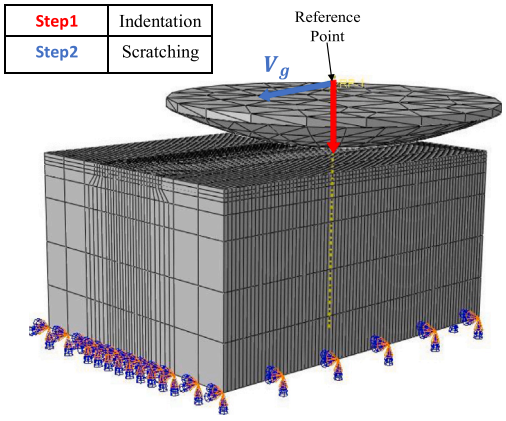

Fig. 4. Model for Lagrangian method.

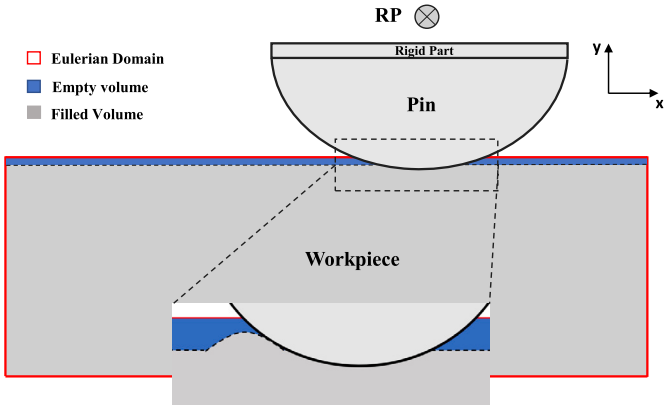

Fig. 5. Model for CEL method.

4.3.2. CEL « Coupled-Eulerian–Lagrangian » method

For Eulerian analysis, the nodes of the mesh are typically fixed in space, allowing the material to deform and move freely through the elements. Eulerian mesh is constructed to extend well beyond the boundaries of the Eulerian material. Eulerian–Lagrangian contact allows the Eulerian material to interact easily with Lagrangian elements. In the case of large deformations, Eulerian analyses are effective, unlike Lagrangian. To simulate the friction test using the "CEL" technique, an Eulerian space is created, which is the zone of the plastic deformation of the material. Part of this domain will be filled with the material (Ti–6Al–4V), while another part remains empty. The principle of pin motion is similar to the Lagrangian method, the simulation is divided into two steps: Indentation and scratching. When the pin moves horizontally, it causes plowing due to the plastic deformation of the material, as shown in Fig. 5. The Eulerian material flows easily through the mesh elements [26,27].

4.3.3. Arbitrary-Lagrangian-Eulerian (ALE) method

The adaptive meshing technique combines the advantages of both pure Lagrangian and pure Eulerian analyses. This type of adaptive mesh is commonly referred to as "Arbitrary-Lagrangian–Eulerian" (ALE). ALE allows the mesh to move independently of the material. To perform an analysis using the ALE technique, an adaptive mesh domain needs to be defined, which can be either Eulerian or Lagrangian. In general, the mesh is not fixed in space, so mesh constraints must be defined to prevent it from moving along with the material. This approach is based on modeling the relative movement between the pin and the workpiece as if it were a fluid flow [26,27]. The material flows through the part of a well-defined sliding speed (V_g), while the pin remains fixed, as presented in Fig. 6.

4.3.4. Numerical simulation

The friction test was simulated using three different methods to facilitate a comparative analysis of the results, thereby determining the most relevant approach. All three models are identical in terms of size and the number of elements, as detailed in Table 5. The indentation depth was set at 30 μm, and the scratching distance covered was 2 mm. The sliding speed (V_g) was fixed at 50 m/min. The friction coefficient, introduced into Abaqus to characterize the mechanical contact, was maintained at 0.1 throughout the simulation.

For each modeling strategy, the normal and tangential forces ($F_{N_{num}}$) and ($F_{T_{num}}$) were recovered and used to calculate the apparent numerical friction coefficient ($\mu_{app_{num}}$) according to the Eq. (1). The Table 6 illustrates the numerical apparent friction coefficients, along with their computing times. The deviation between the friction coefficients is less than 3%. However, there is a significant difference in the computing time. The "Lagrangian" model is 6 times faster than the "CEL" model, and it is 14 times faster than the "ALE" model. This substantial difference in computational time is an important consideration when choosing the appropriate model for a given analysis. This is all the more important as calculating the adhesion coefficient using the inverse method may require a large number of simulations to be run. While the accuracy of the results is comparable among the models, the computational efficiency varies considerably, making the Lagrangian model a more efficient choice for simulating the friction test.

5. Determination of adhesive friction coefficient

The methodology of determining the adhesive friction coefficient (μ_{adh}) involved a systematic approach comprising several sequential steps. Initially, experimental friction tests were conducted under conditions detailed in Table 1 to determine apparent friction coefficients. Subsequently, numerical simulations were performed to obtain the

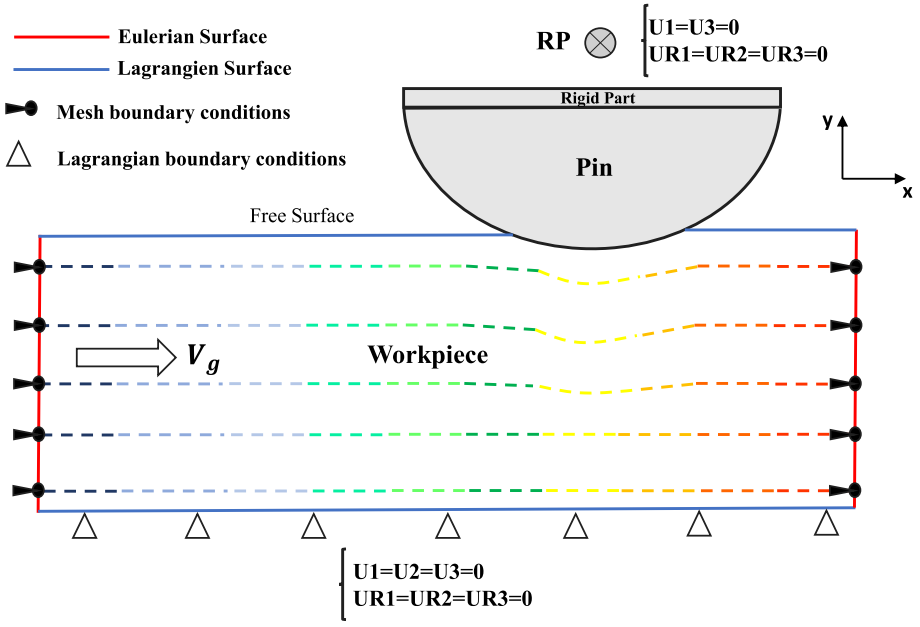

Fig. 6. Model for ALE method [16].

Table 5
Simulation parameters.

	Parameter	CEL	ALE	Lagrangian
Workpiece	Size (mm)	0.05 0.5	0.05 0.5	0.05 0.5
	Type	C3D8R	C3D8R	C3D8R
	Number	819	819	819
Pin	Size (mm)	0.4	0.4	0.4
	Type	C3D4	C3D4	C3D4
	Number	819	819	819
Rigid part	Size (mm)	0.6	0.6	0.6
	Type	C3D4	C3D4	C3D4
	Number	230	230	230

Table 6
Numerical friction coefficient and computing time.

Model	Numerical friction coefficient	Computing time
Lagrangian	0.122	2 h and 15 min
CEL	0.125	14 h
ALE	0.127	33 h

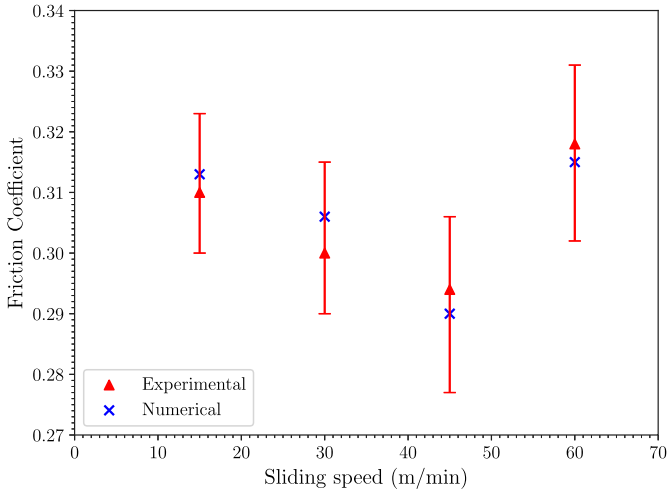

Fig. 7. Comparison between numerical and experimental friction coefficients.

experimental normal force ($F_{N_{exp}}$) of 350 N. These simulations indicated that maintaining a consistent indentation depth of the pin into the material (h = 11.7 μm) was necessary to reach the target value. Following this, additional numerical simulations were performed to ensure alignment between the numerical and experimental friction coefficients ($\mu_{app-num} \approx \mu_{app-exp}$), by adjusting the adhesive friction coefficient (μ_{adh}) implemented in Abaqus.

The final results, as illustrated in Fig. 7, provide a comparative analysis between the experimental and numerical friction coefficients. Notably, the figure reveals a deviation of less than 5%, indicating a relatively close alignment between the two sets of data. Despite this close agreement, there exist minor disparities between the friction coefficients derived from experimental tests and those obtained through numerical simulations. These differences, although slight, may arise from various factors such as material properties, surface conditions, or the inherent limitations of the simulation model. Nevertheless, the overall consistency between the experimental and numerical results suggests that the numerical model adequately represents the real-world behavior of the system under study.

The aim is to determine the adhesive friction coefficient for each sliding velocity. The proportion of the adhesive friction and the plastic deformation in the apparent friction coefficient is shown in Fig. 8, it appears that the proportion of the plastic deformation is always lower than 5%. On the other hand, the adhesion coefficient represents more than 95% of the apparent friction coefficient. This distribution remains the same regardless of the friction speed. This result shows that for our case study, the apparent friction coefficient measured experimentally with the tribometer corresponds mainly to the adhesive friction coefficient (real coefficient of friction) between the two materials. In the rest of the study, only the apparent friction coefficient will be considered.

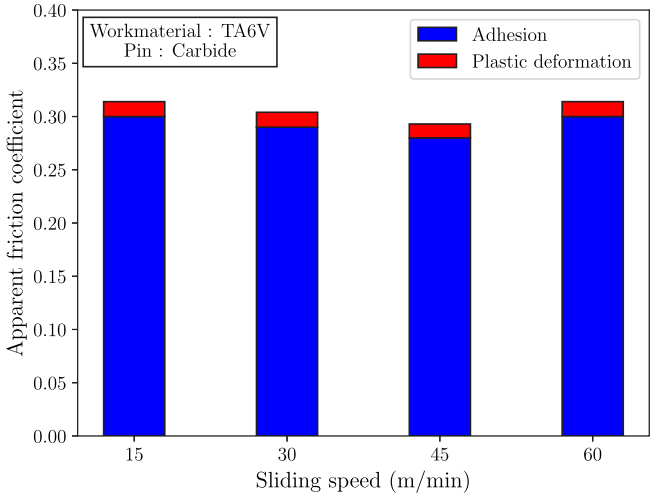

Fig. 8. Proportion of adhesion and plastic deformation; dry friction.

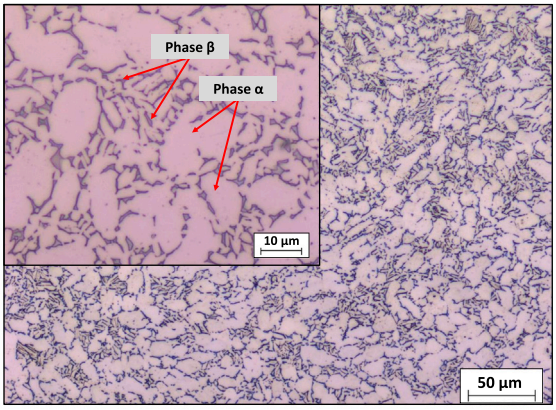

Fig. 9. Micro-structure of Ti–6Al–4V.

Table 7
Mechanical properties of Ti–6Al–4V (material manufacturer: TIMET).

Rm (MPa)	Rp 0.2% (MPa)	A %	Hardness (HRC)	Hardness (HB)
937	873	21.5	33	321

Table 8
Chemical composition of Ti–6Al–4V (material manufacturer: TIMET).

Element	C	V	N	Fe	Ti	Al	H	O
Mass percentage %	0.014	4.25	0.008	0.14	88.89	6.53	0.002	0.166

6. Experimental set-up

6.1. Investigated materials

The workpiece (Ti–6Al–4V) has a diameter of 90 mm and a length of 150 mm. Its mechanical properties are outlined in Table 7, while its chemical composition in terms of mass fraction is provided in Table 8. The titanium alloy ($\alpha + \beta$) exhibits a duplex microstructure, which is characterized by primary α grains with a hexagonal close-packed (hcp) structure, surrounded by transformed β grains with a body-centered cubic (bcc) structure (Fig. 9). The cylindrical pin has a spherical extremity ($\varnothing 9mm$). It is made of sintered tungsten carbide with a similar grade as that used for cutting tools designed for machining the titanium alloys. The surface of the pin has been polished to get a similar surface finishing as a cutting face of the tool.

6.2. Lubrication conditions

The tests were carried out under different conditions: dry, emulsion and cryogenic.

6.2.1. Emulsion

The pin/workpiece interface is lubricated using a cutting fluid (ECOCOOL CS+) with a 6% oil concentration in the emulsion. This fluid is directed onto the contact zone through an 8 mm diameter nozzle.

6.2.2. Cryogenic assistance (LN2)

Liquid nitrogen (LN2) is projected onto the pin/workpiece contact zone through a 2 mm diameter nozzle at a pressure of 12 bar, with a flow rate of 2.95 L/min. The cryogenic fluid is stored in a 180-liter tank and supplied to the contact zone through insulated thermal pipes. The flow rate is measured by connecting the nitrogen tank to an HBM S9M/5KN load cell, which records its weight. The Fig. 10 depicts the weight versus time, showing a linear decrease in effort. The slope of the curve is utilized to calculate the nitrogen mass flow rate, which is determined to be 2.38 kg/min, corresponding to a flow rate of 2.95 L/min.

7. Experimental results

In this section, the results of the experimental trials have been analyzed. The analyses concern the impact of sliding speed and the friction condition on the apparent friction coefficient.

7.1. Impact of sliding velocity (V_g)

Fig. 11 presents the evolution of experimental apparent friction coefficient versus the sliding speed for the three configurations. The results obtained clearly demonstrate that the experimental apparent friction coefficient ($\mu_{app-exp}$) varies as the sliding speed (V_g) increases. The friction coefficient exhibits similar trends across all tested conditions, revealing two distinct behaviors. Initially, below a sliding speed of 45 m/min, the friction coefficient gradually decreases until it reaches a minimum value. However, at sliding speeds from 45 m/min to 90 m/min, the friction coefficient starts to increase.

The results are consistent with those reported by Meier et al. [28], who exhibited a similar trend in the friction coefficient versus the sliding speed. Their study investigated the friction behavior of a carbide pin with Ti–6Al–4V under both dry and lubricated conditions. They attributed the increase in the friction coefficient to the formation of an adhesive layer of titanium on the pin's surface, providing insight into the observed behavior. Makich et al. [29] obtained similar results when investigating the friction behavior of Ti–6Al–4V under various friction conditions, including both dry and cryogenic environments. They noted an increase in the friction coefficient at higher sliding velocities (60 m/min) during cryogenic friction. The authors explained that the cryogenic temperature caused embrittlement of the asperities, particularly at higher sliding velocities. Consequently, this embrittlement led to more pronounced shock on the asperities, resulting in higher friction coefficients.

The studies conducted by Courbon et al. [10] and Bonnet et al. [13], investigating the friction of Ti–6Al–4V against carbide tools, both observed a decrease in the apparent friction coefficient as the sliding speed increased. However, variations in the results could be attributed to differences in the applied normal forces on the pin (1000 N), which consequently affect the contact pressure.

To better understand the phenomena occurring at the pin/workpiece interface, a chemical analysis using an Energy-Dispersive X-ray Spectroscopy (EDS) device, was conducted on the surface of the pin under all investigated friction conditions, as presented in Fig. 12. The results indicate that titanium adheres to the surface of the carbide pin, serving as an indicator of the adhesion phenomenon.

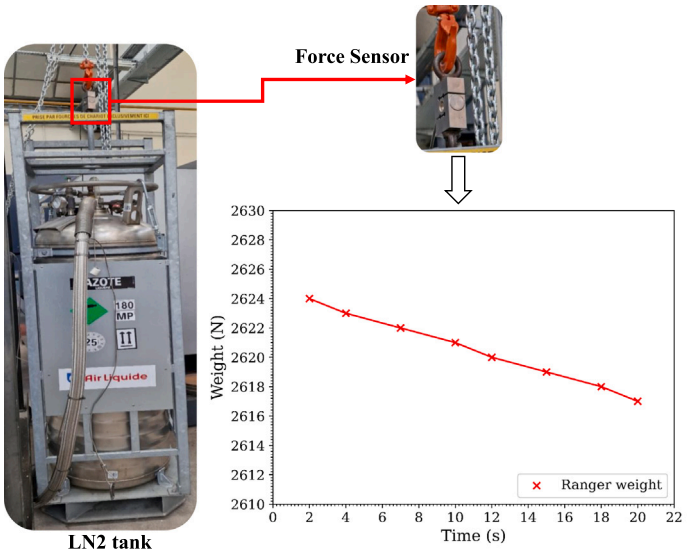

Fig. 10. Flow rate measure.

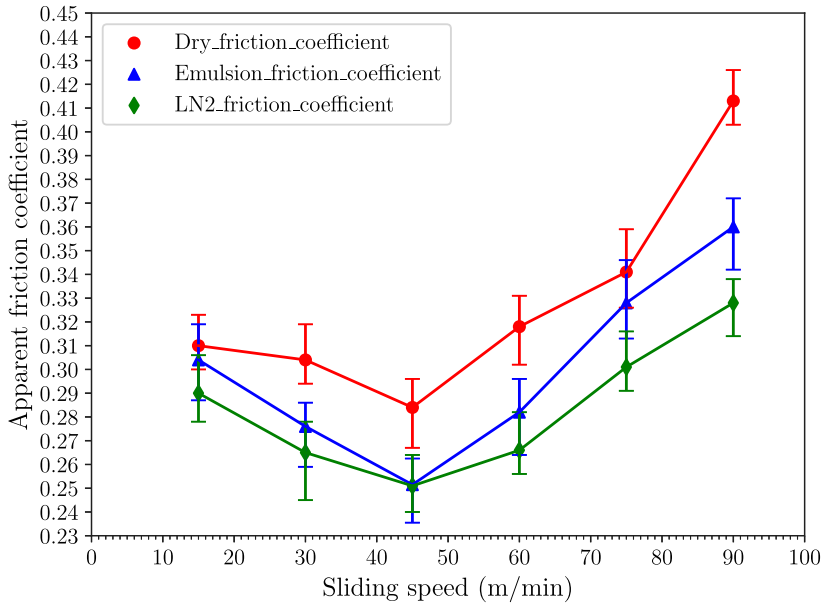

Fig. 11. Evolution of the friction coefficient by sliding speed.

Notably, as the sliding speed increases, a higher quantity of titanium becomes adhered. At sliding speeds of 75 m/min and 90 m/min, an adhesion layer forms and binds to the pin surface. Furthermore, the nature of the lubrication influences significantly the quantity of adhered titanium.

The observations from the EDS analysis are in line with previous studies. Makich et al. [29] observed that the cryogenic bath limitd the adhesion phenomenon and reduced the worn surface by 85%. Similarly, the authors of the study [30] revealed that the use of Liquid Carbon Dioxide (LCO2) and lubrication fluid or Minimum Quantity Lubrication (MQL) reduced the contact area by 25% and 35% respectively compared to dry friction. These researchers have confirmed that the nature of lubrication influences significantly the quantity of adhered titanium., whether conventional (emulsion) or with cryogenic fluids, restricts the phenomenon of adhesion compared to dry.

7.2. Effect of lubrication fluid

The results presented in Fig. 11, highlight the significant influence of the lubrication fluid employed during friction tests on the apparent friction coefficient ($\mu_{app-exp}$). The introduction of a lubricating fluid at the pin/workpiece interface profoundly affects the tribological behavior of the studied materials. The fluid forms a lubricating film between the two surfaces, effectively preventing direct contact between surface asperities. This lubricated contact between the workpiece and the pin results in a reduction of the apparent friction coefficient. These results are consistent with the study conducted by Meier et al. [28], who explained that ester oil forms an adsorption layer between the surfaces, leading to a decreased friction coefficient when compared to dry friction.

The results depicted in Fig. 11 demonstrate that cryogenic assistance using liquid nitrogen (LN2) has a significant effect on the tribological

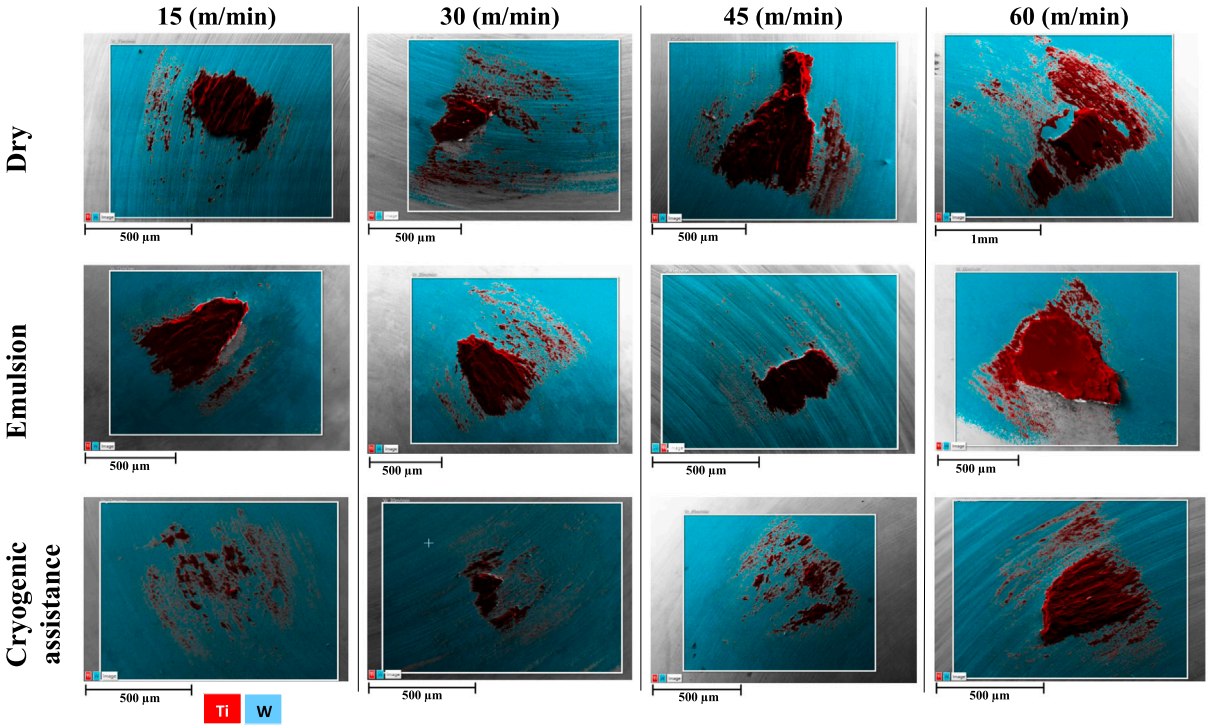

Fig. 12. EDS analyze on the pin's surface.

behavior of Ti–6Al–4V against tungsten. At atmospheric pressure, the liquid nitrogen (LN2) boils at a temperature of (−196 °C) which leads to a transformation from a liquid to a gaseous state. This transformation generates low temperatures at the pin/workpiece, consequently influencing the coefficient of friction. The directed application of cryogenic fluid to the contact zone results in a noticeable reduction in the apparent friction coefficient compared to using a classic lubrication fluid. These results are consistent with those of Makich et al. [29]. The authors noted a reduction in the friction coefficient with the use of liquid nitrogen (LN2) compared to dry friction. However, contradictory findings were reported by Courbon et al. [10,14], who investigated the impact of cryogenic fluids on the friction characterization of Ti–6Al–4V. They concluded that the utilization of cryogenic assistance with LN2, LCO2, or LCO2 + MQL did not affect the friction coefficient.

Pušavec et al. [11] investigated the impact of various lubrication conditions on the friction coefficient. Their study revealed that using liquid carbon dioxide (LCO2) resulted in an increase in the friction coefficient compared to using an emulsion. However, the combination of oil with LCO2 resulted in a notable reduction of friction coefficients. The researchers attributed these findings to the lubricating effect of the added oil, facilitating the formation of a tribofilm between the surfaces, while LCO2 primarily exerted a cooling effect.

8. Discussion

Based on the obtained results, it appears that extreme contact conditions, such as high pressure and temperature, result in the phenomenon of adhesion, where a layer of titanium adheres to the surface of the pin during friction tests. When the sliding speed (V_g) increases from 15 m/min to 45 m/min, the titanium adhering to the pin's surface does not change the nature and contact conditions. However, the increase of sliding speed generates more heat at the pin/workpiece interface due to friction. These results confirm those of several previous works such as Bonnet et al. [22], Courbon et al. [10] and Egana et al. [31]. The elevated temperature in the contact zone causes a rise in temperature at the deformed region of the material, leading to a modification of its mechanical properties. Consequently, the material becomes more sensitive to deformation, and it easily flows along the edges of the pin. However, if the sliding speed (V_g) exceeds 45 m/min, the amount of titanium adhered to the pin tip becomes significant. This adherence leads to a transformation of the contact from carbide/titanium to titanium/titanium. The shearing between the adhered titanium and the titanium of the workpiece contributes to an increase in tangential forces, resulting in an apparent increase in the friction coefficient. There is a critical threshold for the friction speed, beyond which the adhesion phenomenon becomes significant and begins to influence the nature of the contact, particularly the coefficient of friction. During the machining process, adhesion can lead to the formation of a 'built-up edge.' The presence of a lubrication fluid has a notable impact on the friction behavior by effectively reducing the friction coefficient. Moreover, injecting liquid nitrogen into the contact zone between titanium and tungsten lead to lower the temperature. The decreased temperatures in the contact zone serve to restrict the adhesion of titanium, which tends to occur at elevated temperatures. Consequently, the shear forces between the adhered portion and the workpiece are less pronounced, resulting in a reduction of the friction coefficient, of the order of 5% compared to emulsion and 12% compared to dry machining. The comparison between numerical and experimental results has revealed a notably close correspondence with the observed difference (less than 5%). This disparity confirms a robust agreement between numerical simulations and experimental tests. The correlation between these two datasets serves to validate the numerical model employed for simulating the friction test.

9. Conclusion

This article has characterized the friction behavior of Ti–6Al–4V with tungsten carbide tools under dry, lubricated, and cryogenic machining conditions. A specialized tribometer was used to replicate analogous tribological phenomena occurring at the tool-chip-workpiece interface during metal cutting. This involves high contact pressures (approximately 1.5 GPa) and several sliding speeds (60–90 m/min). To calculate the real friction coefficient (adhesive coefficient), it was demonstrated that a Lagrangian numerical simulation was the most

relevant. The obtained results highlighted that the friction coefficient is influenced by variations in sliding speed. Under such friction conditions (high temperature and contact pressure), titanium exhibits significant adhesion, significantly affecting the nature of contact and influencing the friction coefficient. There exists a critical sliding speed threshold, approximately 45 m/min, beyond which the adhesion phenomenon becomes significant. The use of cutting fluid emulsion reduces the friction coefficient by (5%) compared to dry friction. Furthermore, friction under cryogenic conditions (using LN2) further decreases the friction coefficient by 12%. This reduction in the friction coefficient, along with the decrease in the cutting zone temperature, may explain the increased tool lifespan when using cryogenic fluid.

CRediT authorship contribution statement

Achraf Fersi: Writing – original draft, Investigation, Formal analysis. **Yessine Ayed:** Supervision. **Bruno Lavisse:** Supervision. **Guénaël Germain:** Supervision.

Declaration of competing interest

The authors declare that they have no known competing financial interests or personal relationships that could have appeared to influence the work reported in this paper.

Data availability

Data will be made available on request.

Acknowledgments

The authors express their gratitude to the Cetim, and all the esteemed partners involved in the ScCRYO2 project, as well as the Carnot ARTS Institute, the Pays de la Loire Region and Angers Loire Métropole for their financial support.

References

[1] Du Z, Xiao S, Xu L, Tian J, Kong F, Chen Y. Effect of heat treatment on microstructure and mechanical properties of a new β high strength titanium alloy. Mater Des 2014;55:183–90.
[2] Arab A, Chen P, Guo Y. Effects of microstructure on the dynamic properties of TA15 titanium alloy. Mech Mater 2019;137:103121.
[3] Hoyne AC, Nath C, Kapoor SG. On cutting temperature measurement during titanium machining with an atomization-based cutting fluid spray system. J Manuf Sci Eng 2015;137(2):024502.
[4] Ayed Y, Germain G, Melsio AP, Kowalewski P, Locufier D. Impact of supply conditions of liquid nitrogen on tool wear and surface integrity when machining the Ti-6Al-4V titanium alloy. Int J Adv Manuf Technol 2017;93:1199–206.
[5] Agrawal C, Wadhwa J, Pitroda A, Pruncu CI, Sarikaya M, Khanna N. Comprehensive analysis of tool wear, tool life, surface roughness, costing and carbon emissions in turning Ti–6Al–4V titanium alloy: Cryogenic versus wet machining. Tribol Int 2021;153:106597.
[6] Bogdan-Chudy M, Niesłony P, Gupta MK, Wojciechowski S, Maruda RW, Gawlik J, Królczyk GM. Tribological and thermal behavior with wear identification in contact interaction of the Ti6Al4V-sintered carbide with AlTiN coatings pair. Tribol Int 2022;167:107394.
[7] Uçak N, Outeiro J, Aslantas K, Çiçek A, Çetin B. Determination of the friction coefficients between uncoated WC-Co tools and L-PBF and wrought Ti-6Al-4V alloys for micro-milling simulations. Proc. CIRP 2023;117:281–6.
[8] Basten S, Seis L, Oehler M, Kirsch B, Hasse H, Aurich JC. Tribological behaviour of AISI 4140 and WC-Co carbides during dry condition, using cryogenic media, and sub-zero metalworking fluids at high contact stresses. Wear 2023;512:204525.
[9] Schulze V, Bleicher F, Courbon C, Gerstenmeyer M, Meier L, Philipp J, Rech J, Schneider J, Segebade E, Steininger A, et al. Determination of constitutive friction laws appropriate for simulation of cutting processes. CIRP J. Manuf. Sci. Technol. 2022;38:139–58.
[10] Courbon C, Pusavec F, Dumont F, Rech J, Kopac J. Tribological behaviour of Ti6Al4V and Inconel718 under dry and cryogenic conditions—Application to the context of machining with carbide tools. Tribol Int 2013;66:72–82.
[11] Pušavec F, Sterle L, Kalin M, Mallipeddi D, Krajnik P. Tribology of solid-lubricated liquid carbon dioxide assisted machining. CIRP Ann. 2020;69(1):69–72.
[12] Smolenicki D, Boos J, Kuster F, Roelofs H, Wyen CF. In-process measurement of friction coefficient in orthogonal cutting. CIRP Ann. 2014;63(1):97–100.
[13] Bonnet C, Rech J, Poulachon G. Characterization of friction coefficient for simulating drilling contact for titanium TiAl6V4 alloy. CIRP J. Manuf. Sci. Technol. 2020;29:130–7.
[14] Courbon C, Sterle L, Cici M, Pusavec F. Tribological effect of lubricated liquid carbon dioxide on TiAl6V4 and AISI1045 under extreme contact conditions. Procedia Manuf 2020;47:511–6.
[15] Zemzemi F, Rech J, Ben Salem W, Dogui A, Kapsa P. Development of a friction model for the tool-chip-workpiece interfaces during dry machining of AISI4142 steel with TiN coated carbide cutting tools. Int J Mach Mach Mater 2007;2(3–4):361–77.
[16] Abdelali HB, Claudin C, Rech J, Salem WB, Kapsa P, Dogui A. Experimental characterization of friction coefficient at the tool–chip–workpiece interface during dry cutting of AISI 1045. Wear 2012;286:108–15.
[17] Bowden FP, Tabor D. The friction and lubrication of solids. Vol. 1, Oxford University Press; 2001.
[18] Sima M, Özel T. Modified material constitutive models for serrated chip formation simulations and experimental validation in machining of titanium alloy Ti–6Al–4V. Int J Mach Tools Manuf 2010;50(11):943–60.
[19] Karpat Y. Temperature dependent flow softening of titanium alloy Ti6Al4V: An investigation using finite element simulation of machining. J Mater Process Technol 2011;211(4):737–49.
[20] Ramirez C. Critères d'optimisation des alliages de TITane pouraméliorer leur USinabilité (Ph.D. thesis), Paris, ENSAM; 2017.
[21] Zemzemi F, Rech J, Salem WB, Dogui A, Kapsa P. Identification of a friction model at tool/chip/workpiece interfaces in dry machining of AISI4142 treated steels. J. Mater. Process. Technol. 2009;209(8):3978–90.
[22] Bonnet C, Valiorgue F, Rech J, Hamdi H. Improvement of the numerical modeling in orthogonal dry cutting of an AISI 316L stainless steel by the introduction of a new friction model. CIRP J. Manuf. Sci. Technol. 2008;1(2):114–8.
[23] Rech J, Claudin C, D'eramo E. Identification of a friction model—application to the context of dry cutting of an AISI 1045 annealed steel with a TiN-coated carbide tool. Tribol Int 2009;42(5):738–44.
[24] Cao J. Towards a new methodology to identify friction models under severe contact conditions (Ph.D. thesis), Université de Lyon; 2021.
[25] Fezai N, Chaabani L, Niang N, Haamsir MB, Fontaine M, Gilbin A, Picart P. Characterization of friction for the simulation of multi-pass orthogonal micro-cutting of 316L stainless steel. Proc. CIRP 2022;108:845–50.
[26] Benson DJ. Computational methods in Lagrangian and Eulerian hydrocodes. Comput. Methods Appl. Mech. Eng. 1992;99(2–3):235–394.
[27] Simulia DS. Abaqus/CAE user's guide. 2016.
[28] Meier L, Schaal N, Wegener K. In-process measurement of the coefficient of friction on titanium. Proc. CIRP 2017;58:163–8.
[29] Makich H, Nouari M, et al. Effect of cryogenic friction conditions on surface quality. Proc. CIRP 2022;108:675–80.
[30] Sterle L, Pušavec F, Kalin M. Determination of friction coefficient in cutting processes: Comparison between open and closed tribometers. Proc. CIRP 2019;82:101–6.
[31] Egana A, Rech J, Arrazola P. Characterization of friction and heat partition coefficients during machining of a TiAl6V4 titanium alloy and a cemented carbide. Tribol. Trans. 2012;55(5):665–76.